Results in Engineering 28 (2025) 107881

Contents lists available at ScienceDirect

Results in Engineering

journal homepage: www.sciencedirect.com/journal/results-in-engineering

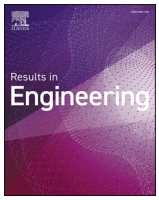

Performance of 3D-structured grinding wheels with multi-layer internal cooling channels

Sharlane Costa [a,b,c], Paulina Capela [a,b,d], Amauri Hassui [e], João Ribeiro [c,*], Mário Pereira [f], Delfim Soares [a,b]

[a] CMEMS - Center for MicroElectromechanical, University of Minho, 4800-058 Guimarães, Portugal
[b] LABBELS – Associate Laboratory, Braga/Guimarães, Portugal
[c] Centro de Investigação de Montanha (CIMO), Instituto Politécnico de Bragança, Campus S. Apolónia, 5300-253 Bragança, Portugal
[d] MEtRICs, Mechanical Eng. Dep., Univ. of Minho, Campus de Azurém, Guimarães, Portugal
[e] Department of Manufacturing and Materials Engineering, School of Mechanical Engineering, University of Campinas – UNICAMP, 13083-860, Campinas, São Paulo, Brazil
[f] Centro de Física das Universidades do Minho e do Porto, Braga, Portugal

ARTICLE INFO

Keywords:
Structured grinding wheel
Grinding temperature
Tribological performance
Sustainable manufacturing
High-efficiency grinding
Internal cooling channels

ABSTRACT

Grinding is a key machining process in industries that demand high precision and surface quality. However, the conventional flood cooling method is often ineffective due to the air barrier formed by the rotating wheel, which restricts fluid access to the contact zone. This causes thermal instability, high coolant use, and environmental impact. To overcome these limitations, this study investigates alumina grinding wheels with internal cooling systems, fabricated by a novel additive route. Sacrificial 3D-printed polymer inserts were embedded during pressing and eliminated during sintering, enabling multilayered channels within a monolithic abrasive matrix. This represents the first practical application, with detailed method of production, of a fully embedded cooling system in vitrified grinding wheels. Two configurations, with one and three internal channel layers, were compared to a conventional wheel under external cooling. Controlled grinding tests on AISI 1045 steel were performed at varying depths of cut, and key variables such as cutting forces, force ratio, specific energy, and temperature variation (ΔT) were analyzed. The three-layer wheel showed the best performance, reducing tangential force by up to 49.3 %, force ratio by 21.3 %, specific energy by 50 %, and ΔT by 58.6 % compared to the conventional system. A detailed thermal profile enabled segmentation into cut-in, steady-state, and cut-out zones. The greatest benefit from internal cooling occurred in the steady-state region, with heating rates reduced by up to 78 %. These results confirm that the proposed additive manufacturing approach offers a scalable route to produce structured wheels with embedded channels, improving coolant application, process stability, and sustainability in high-performance grinding.

Introduction

Grinding is one of the most widely used machining processes for achieving high-precision surfaces [1]. However, the intense contact between the abrasive wheel and the workpiece generates significant heat in the contact zone, which may lead to surface burns, thermal cracks, metallurgical changes [2], increased grinding forces, and accelerated wheel wear [3].

Cutting fluids play a key role in mitigating these issues by promoting heat dissipation, lubricating the interface, and assisting chip evacuation [4]. The most common strategy is external flood cooling, where large volumes of coolant are directed at the grinding zone [5,6]. Despite its widespread use, this method presents critical drawbacks, including excessive fluid use and limited cooling efficiency due to the formation of an air barrier, an aerodynamic layer generated by the rotating wheel that obstructs fluid access to the contact zone [7].

As illustrated in Fig. 1, this air barrier acts as a shield that deflects the fluid stream, especially under high-speed conditions. Effective penetration requires the fluid to overcome the momentum of the rotating air, which is not always achievable, particularly in low-pressure or sustainability-driven setups [8–11].

In addition to technical limitations, conventional flood cooling raises

* Corresponding author.
E-mail addresses: scosta@dem.uminho.pt (S. Costa), jribeiro@ipb.pt (J. Ribeiro).

https://doi.org/10.1016/j.rineng.2025.107881
Received 27 July 2025; Received in revised form 13 October 2025; Accepted 21 October 2025
Available online 22 October 2025

important concerns related to environmental sustainability and operator health [12]. The high volume of cutting fluids used in grinding leads to increased costs for storage, filtering, and disposal, while also generating chemical residues that can contaminate soil and water if not properly treated [13]. Moreover, prolonged exposure to coolant mist and degraded fluids has been associated with dermatological issues, respiratory irritation, and the proliferation of bacteria in the working environment [14]. These factors have driven the development of alternative lubrication strategies that aim to reduce fluid consumption and minimize occupational risks without compromising process efficiency [15].

To overcome these limitations, alternative lubrication strategies have been explored in recent years, including Minimum Quantity Lubrication (MQL) [16–18], cryogenic cooling [19], and the development of textured grinding wheels [20–24]. Although these strategies have shown partial improvements, they present inherent limitations. MQL typically reduces grinding temperature by 20–40 %, tangential and normal forces by 15–35 %, and specific grinding energy by up to 25–30 % compared with conventional flood cooling [17,25–27]. Cryogenic cooling can achieve temperature reductions of 40–60 % and extend tool life by 30–50 %, yet it provides limited lubrication and requires costly pressurization and delivery systems, which restricts its industrial adoption [17,28,29]. Hybrid strategies such as Cryo-MQL further enhance tribological and thermal behavior, lowering cutting temperatures by up to 45 %, surface roughness by 25–40 %, and specific energy by approximately 45 %, but they still demand complex setups and may raise concerns regarding aerosol generation and operator safety [17,27].

Most research on textured grinding wheels has focused on surface-level modifications intended to improve coolant access and chip evacuation [30]. One such approach was demonstrated by Zhang et al. (2024) [31] who applied abrasive waterjet (AWJ) dressing to produce surface textures on diamond grinding wheels. This method enabled simultaneous dressing and texturing, generating precise grooves without thermal damage, and contributing to enhanced tribological performance. Barmouz and Azarhoushang (2025) [32] used digital light processing (DLP) to manufacture hybrid-bond grinding wheels with grooves incorporated directly during printing. These features improved coolant penetration, minimized clogging, and enhanced both surface finish and grinding efficiency. In addition, the tailored hybrid bond composition offered increased thermal stability and wear resistance, demonstrating how adititive manufacturing (AM) enables simultaneous structural and material-level optimization.

Laser-based methods have also shown promise. Xie et al. (2024) [33] employed CO_2 laser ablation to texture the surface of resin-bond diamond wheels, investigating the relationship between process parameters and thermal effects. Their results showed that carefully controlled laser input could create precise grooves without damaging the abrasive structure. The resulting textures improved heat dissipation and chip removal, confirming laser ablation as a precise, non-contact technique for surface functionalization. A more autonomous solution was proposed by Surendran and Sooraj (2025) [34], who developed a sweating-type grinding wheel with an interconnected porous network capable of releasing lubricant in response to rising cutting temperatures and speeds. Manufactured via additive processes, this wheel dispenses fluid without the need for external pumping systems. The self-regulating mechanism effectively reduced forces and temperature, while minimizing fluid consumption, offering a smart, energy-free alternative for sustainable lubrication.

While all these approaches rely on surface-level or near-surface modifications to enhance lubrication [35], an emerging strategy involves integrating internal channels that deliver fluid directly from the wheel center to the cutting zone. This internal cooling approach overcomes the air barrier formed by rotation, enhances heat dissipation, and reduces fluid waste by ensuring localized and effective coolant delivery [36–39]. As a result, internal channels simultaneously overcome the limited cooling capacity of MQL, avoid the clogging issues of surface textures, and provide a more industrially viable solution than cryogenic systems. This makes them a robust and scalable strategy for high-performance grinding.

Most research on grinding wheels with internal channels focuses on the development of pressurized internal cooling systems (Fig. 2a) primarily designed for specific applications such as the grinding of superalloys or other hard-to-machine materials [40,41]. These wheels, often composed of detachable abrasive rings and pressurized fluid systems, have been extensively investigated. In contrast, alumina-based vitrified wheels remain the predominant choice for grinding ferrous alloys in automotive and general engineering industries, owing to their lower cost and versatility compared to superabrasive tools [42–44]. In these applications, strict thermal control is critical to avoid burns and dimensional deviations, yet few studies have addressed how internal channels could improve their performance [45]. On the other hand, little research has been conducted on the application of internal channels in alumina-based vitrified wheels specifically designed for surface grinding of ferrous materials, a process that also demands high dimensional accuracy and strict thermal control [46].

Some promising attempts have been reported in the literature regarding internal coolant delivery in vitrified grinding wheels. Nadolny (2015) [47] developed a small-dimensional "sandwich" grinding wheel equipped with a centrifugal coolant provision system (Fig. 2b) which allowed a fivefold reduction in fluid consumption (from 5.0 to 1.0 L/min) without compromising grinding power or surface quality. However, this approach required the use of a non-abrasive central section for fluid distribution, effectively reducing the active grinding width and limiting the application area. Similarly Sieniawski et al. (2016) [48] tested vitrified grinding wheels containing internal channels and demonstrated good performance in terms of roughness and burn suppression. Nevertheless, the specific fabrication method used to produce the internal supply network was not disclosed, leaving a critical gap in the practical implementation of such systems. This lack of accessible

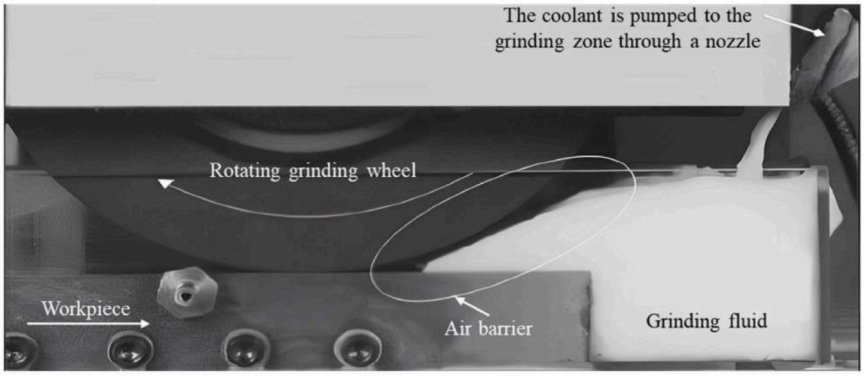

Fig. 1. Air barrier effect during conventional flood cooling in grinding [7,11].

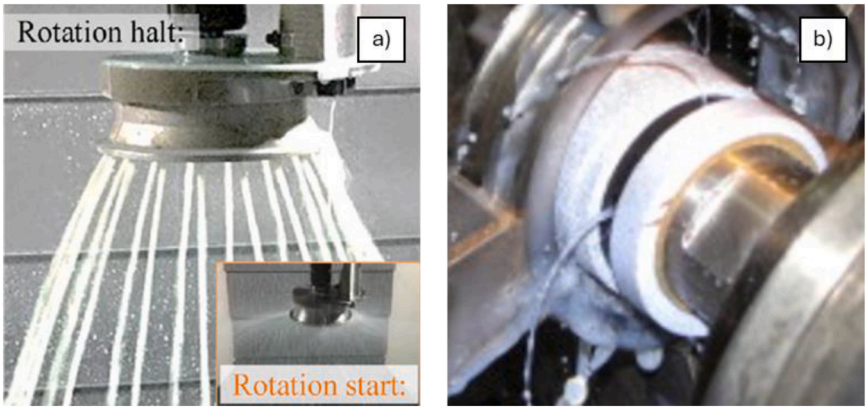

Fig. 2. Examples of internal cooling approaches in grinding wheels. (a) Pressurized system with detachable abrasive rings and centralized fluid injection [36]. (b) Sandwich grinding wheel with centrifugal fluid supply and inactive central core [47].

manufacturing knowledge remains a barrier to the broader adoption of internal cooling configurations in vitrified grinding wheels.

Table 1 summarizes the main grinding parameters and results reported in representative studies that applied internal channel concepts to enhance coolant delivery in surface grinding operations.

These results demonstrate that the use of internal fluid supply can substantially improve cooling efficiency and grinding stability compared with conventional external systems. Reported reductions include up to 30–45 % in tangential forces, 23–35 % in specific grinding energy, and up to 50 % in temperature, while achieving comparable or improved surface quality and reducing fluid consumption by as much as 90 % [47–52]. Such performance is comparable to or even superior to that reported for MQL and Cryo-MQL systems, which typically yield 20–50 % reductions in forces, specific energy and temperatures but require complex and costly delivery infrastructures [17,27].

In this work, an innovative fabrication method is proposed to create fully integrated, three-dimensional internal channels in vitrified alumina grinding wheels specifically designed for internal lubrication. Unlike previous approaches based on machined grooves or detachable pressurized systems, the channels were formed using sacrificial polymer structures produced by 3D printing, which were embedded during pressing and later removed by thermal decomposition during sintering. The radial channels are connected to a central inlet, allowing the fluid to flow through the wheel body and reach the contact zone directly. This configuration represents the first complete and practical application of the technique for embedded fluid delivery in vitrified grinding wheels.

Building upon this manufacturing innovation, the present study evaluates the thermal and tribological performance of the developed structured grinding wheels. Three configurations were compared: a conventional grinding wheel with external flooding, and two structured grinding wheels, with one and three layers of internal channels. In addition to evaluating the average values of cutting force, force ratio, specific energy and temperature variation at different cutting depths, the analysis also included a zone-based assessment of tangential force and temperature, offering a more comprehensive view of process efficiency. This zone-based approach provides a detailed understanding of the temperature evolution and highlights the fluid's role in each grinding phase. The results obtained from these analyses support the development of more efficient and sustainable lubrication strategies, with direct implications for industrial applications requiring strict thermal control and high dimensional accuracy.

Materials and methods

This section details the materials, manufacturing steps, and experimental procedures employed in the development and evaluation of the internally cooled grinding wheels. Emphasis is placed on the novel fabrication method, the design of the lubrication system, and the comparative testing strategy used to assess thermal and tribological performance.

2.1. Grinding wheel fabrication with integrated cooling channels

In this study, a novel fabrication strategy was developed to produce vitrified alumina grinding wheels with embedded radial cooling channels, tailored specifically for internal fluid delivery. The process combined aluminum oxide abrasive grains with a vitreous bonding matrix and integrated sacrificial polymer structures, which were later removed

Table 1
Summary of coolant application strategies with internal supply channels on surface grinding.

Author / Year	Wheel / Workpiece	Channel geometry	Grinding conditions	Flow rate	Main results
Nguyen & Zhang, 2009 [49]	CBN wheel, Ø 300 mm/ AISI 4140 steel	Radial, 144 holes, Ø 2 mm	Vs = 23 m/s; Vw = 400 mm/min; a_e = 10–50 μm	4.8 L/min vs 14.5 L/min (external)	↓ Ft up to 30 %; ↓ Specific energy 23.5 %; ↑ Surface finish
Nadolny, 2015 [47]	Alumina wheel, Ø 35 mm / 100Cr6 steel	Radial, 4 channels, Ø 1.0 mm	Vs = 60 m/s; Vw = 0.75 m/s; a_e = 0.15 mm	1–2 L/min vs 5 L/min (external)	↓ Surface roughness ≈ 30 %; ↓ Grinding power 7–11 %
Sieniawski & Nadolny, 2016 [48,50]	Alumina wheel, Ø 250 mm / CrV12 steel	Radial, 1, 2 and 3 layers (18 channels per layer), Ø 2 mm;	Vs = 30 m/s; Vw = 5–20 m/min; a_e = 0.05 mm	0.5 L/min vs 5 L/min (external)	Internal flood: Improve residual stresses; similar Ft; ↓ Surface roughness. With limiter system: Improve residual stresses; ↓ Ft up to 28 %; Roughness unchanged, but with 90% fluid saving
Barmouz et al., 2023 [51]	SiC wheel, Ø 62 mm / 7075 aluminum alloy	Cylindrical , CP+*S*, Venturi channels; Ø 0.6 mm + slots	Vs = 30 m/s; Vw = 600–6000 mm/min; a_e = 10–100 μm	45 L/min	↓ Ft up to 45 %; ↓ Wheel wear up to 70 %; ↓ Surface roughness up to 30 %
Peng et al., 2025 [52]	CBN wheel, Ø 82 mm / Inconel 718	Slots, 16 channels, Ø 2 mm (parallel, diagonal, V-shaped patterns)	Vs = 3500 rpm; Vw = 800 mm/min; a_e = 20 μm	3–9 L/min	↓ Temperature up to 50 %; ↓ Surface roughness up to 38 %; ↓ Microhardness up to 16.7 %

by thermal decomposition during sintering. Fig. 3 illustrates the main steps of the fabrication process. The polymeric structures were produced by 3D printing and inserted into the mold along with the abrasive powder. After compaction, the green body was subjected to a thermal cycle in a controlled atmosphere. During sintering, the polymer was fully eliminated, resulting in an internal network of radial channels embedded in the vitrified abrasive matrix.

This approach offers a fully embedded solution for fluid delivery, eliminating the need for external pressurization systems or post-processing steps. Unlike conventional grooves produced by machining or laser ablation, this method enables the direct creation of multilayered radial channels throughout the wheel body, all formed in a single sintering cycle.

In a previous study [53], the structural behavior of the sacrificial polymer (PLA) during pressing and sintering was examined in detail. PLA was selected due to its biodegradability, cost-effectiveness, and thermal decomposition below the vitrified bond softening point (~620 °C), ensuring clean channel formation without combustion residues. Thermal analyses (DSC/TGA) confirmed that PLA combustion was completed between 300 and 450 °C, well before matrix densification, thereby preventing contamination of the vitrified structure. Process parameters such as binder content, drying ramp (0.1 °C/min), and pressing conditions (≈27.5 MPa) were optimized to avoid cracking and dimensional instabilities. Dimensional analyses indicated deviations below 5.4 % between the designed and sintered geometries, demonstrating that the method enables the precise and repeatable formation of internal channels without compromising the integrity of the abrasive body.

Building on those findings, the present work adapts the method to implement fully embedded radial channels designed specifically for internal lubrication, expanding the functionality of the structured wheel concept.

Three grinding wheels were produced for this study: a conventional reference wheel without internal channels, designed for external flood cooling, and two structured wheels with embedded radial channels for internal cooling. In these structured wheels, the channels were manufactured with a small forward inclination of $\theta = 102^{\circ}$ measured relative to the workpiece surface (i.e., 12° away from a purely radial outlet at 90° and oriented with the sense of rotation), as identified by a previous CFD Taguchi–Grey optimization [54]. That analysis indicated that this forward inclination helps smooth the discharge from the channel outlet, mitigates local recirculation, and improves coolant penetration into the contact zone when compared with straight radial channels ($\theta = 90^{\circ}$) [55]. It also showed that channel diameter and channel count are the dominant factors for improving fluid availability; therefore, channels of 1.7 mm diameter were adopted, with either one layer of 30 channels at mid-height or three layers totaling 30 channels (10 per layer), with an interlayer spacing of about 2 mm in the multilayer case to preserve distribution along the wheel width.

All wheels had the same outer diameter (62 mm), height (15 mm), and central hole (21 mm). Fig. 4 shows the development process and resulting structures for both designs. CAD models, printed sacrificial structures, and final sintered wheels are presented for comparison between the one-layer and three-layer configurations.

The main geometric parameters of both designs are summarized in Fig. 4, which combines a comparative table (Fig. 5a) with reference images of the sintered wheels (Figs. 5b and 5c) showing the physical meaning of each dimension used in the analysis (d1 to d5).

This structured design represents a key advancement in the application of additive manufacturing principles to traditional ceramic tool fabrication. By enabling internal features to be shaped during the mold stage, it bridges the gap between geometric freedom and industrial scalability, offering a practical path to functional customization in vitrified wheels.

2.2. Internal lubrication system

To validate the effectiveness of the internal channel system under realistic conditions, a dedicated lubrication setup was custom-engineered and integrated into the grinding machine. The coolant is introduced through a stationary inlet and guided along the rotating shaft until it reaches a specially adapted wheel holder equipped with radial outlet ports. These ports feed an internal chamber located between the shaft and the grinding wheel (Fig. 6a). This chamber acts as a pressurized buffer reservoir, ensuring consistent and uninterrupted fluid supply to the base of the internal channels. Once inside the tool, the coolant flows through the radial channel network and exits uniformly at the abrasive surface (Fig. 6b), enabling direct contact with the grinding zone.

Unlike external systems that rely on nozzle positioning and are often affected by fluid deflection due to the air barrier generated at high wheel speeds, this internal configuration ensures consistent and effective coolant delivery directly to the contact zone, even under demanding operating conditions.

2.3. Experimental setup

Fig. 7 presents a schematic of the experimental setup used for the grinding tests, which were conducted under two distinct lubrication strategies: conventional external flood cooling (Fig. 7a) and internal

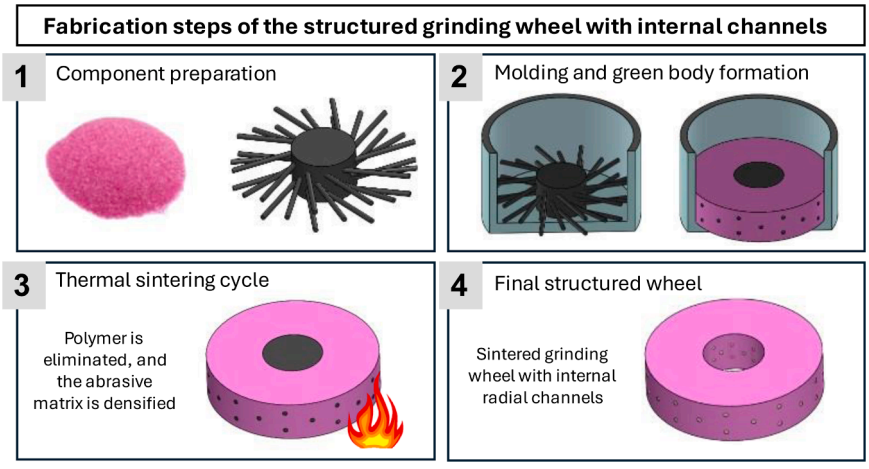

Fig. 3. Fabrication steps of the structured grinding wheel with internal channels: (1) Component preparation; (2) Molding and green body formation; (3) Thermal sintering cycle; (4) Final structured wheel with integrated radial channels.

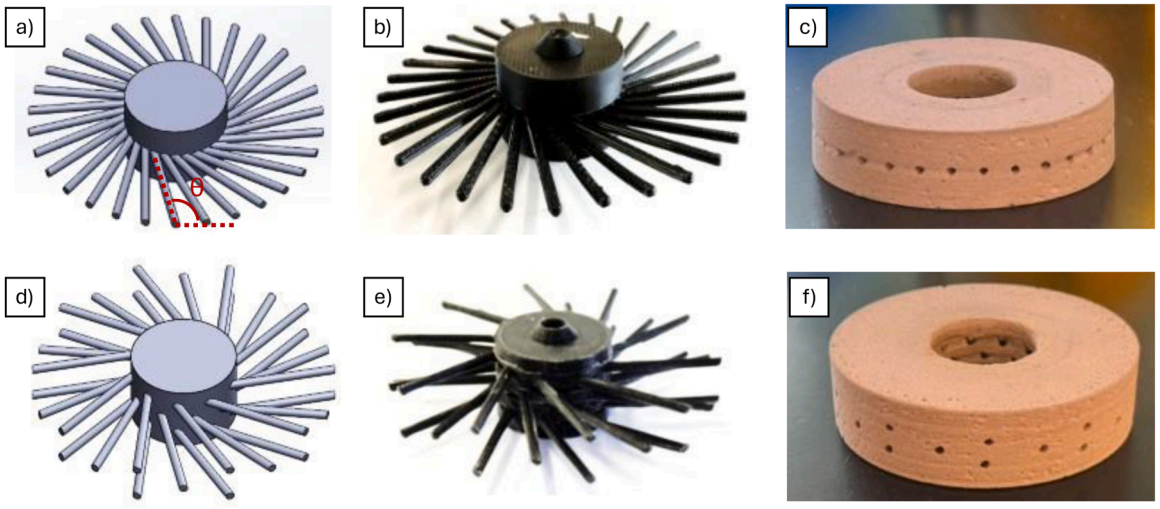

Fig. 4. Development of internally structured grinding wheels with radial channels. (a–c) One-layer configuration: CAD model (a), printed sacrificial structure (b), and vitrified wheel after sintering (c). (d–f) Three-layer configuration: CAD model (d), printed sacrificial structure (e), and vitrified wheel after sintering (f).

a)

Parameter	1 Layer	3 Layers
Number of Channels per layer	30	10
Number of layers	1	3
Channel Diameter (mm)	1.7	1.7
Total Outlet Area (mm ^{2})	68.1	68.1
d1 (mm)	7.5	7.5
d2 (mm)	-	5.5
d3 (mm)	-	4.0
d4 (mm)	6.5	9.7
d5 (mm)	-	19.5

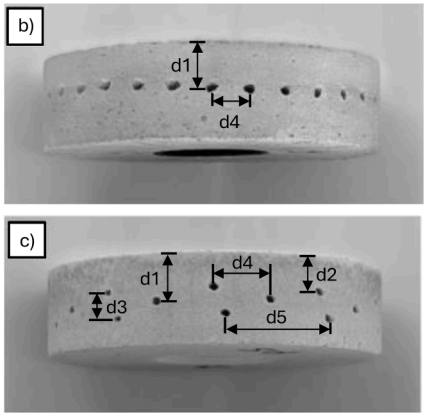

Fig. 5. Geometric characterization of the structured grinding wheels (a) and the dimensional references for the one-layer wheel (b) and for the three-layer wheel (c).

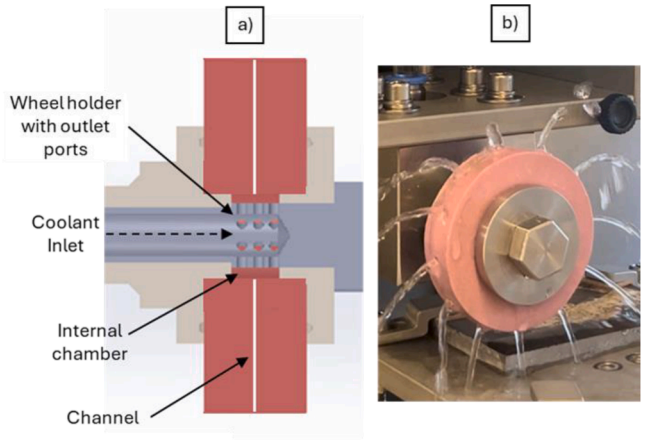

Fig. 6. Internal lubrication system: (a) CAD model of the rotating shaft and wheel holder (Schematic only, scale and geometry not represented); (b) photograph of coolant exiting through the radial channels of the grinding wheel (wheel not rotating).

cooling via structured wheels with radial channels (Fig. 7b). The figure also indicates the direction of wheel rotation, workpiece feed, thermocouple position, and load cell placement.

In the external flooding setup, the cutting fluid was applied through a directional nozzle positioned upstream of the contact zone, as is standard in conventional flood lubrication systems. The nozzle had an outlet area of 15 × 2 mm.

The temperature was acquired using a type K thermocouple, positioned 7.5 mm from the end of the grinding path, as indicated in Fig. 2a. This position corresponds to the midpoint of the workpiece length and is located 1 mm below the surface. Although positioned subsurface, this setup provided a reliable estimation of thermal behavior near the contact zone. Data were recorded at 5 Hz, and the maximum temperature reached during each grinding cycle was used for comparative analysis. The thermocouple was calibrated prior to testing, and the measurements consistently showed reproducible results across repetitions, confirming the reliability of the thermal data.

Cutting forces were recorded using a TAS3F load cell mounted beneath the workpiece holder, enabling simultaneous acquisition of tangential (*Ft*) and normal (*Fn*) forces. The force ratio was adopted as an indicator of the tribological behavior of the system and calculated as shown in Eq. (1):

$$\textit{Force ratio} = \frac{F_t}{F_n} \tag{1}$$

To assess the energy efficiency of the material removal process for each wheel configuration, specific grinding energy (*Ec*) was also calculated according to Eq. (2):

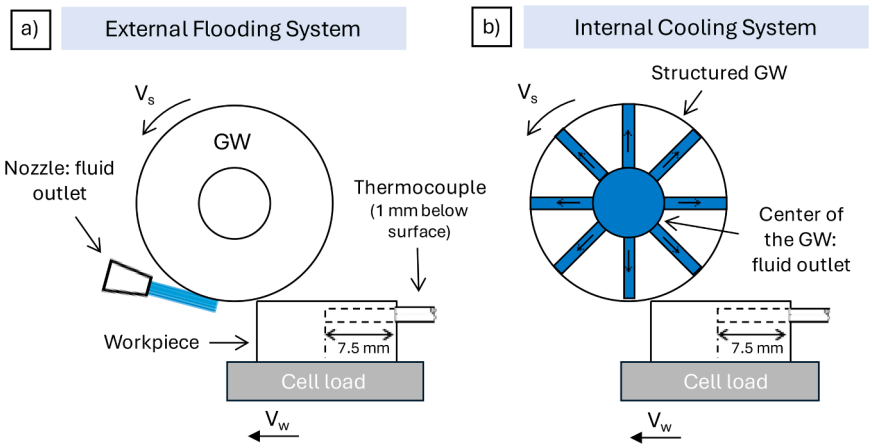

Fig. 7. Schematic representation of the lubrication systems used in the grinding tests: (a) conventional system with external fluid application; (b) internal cooling system using radial channels embedded in the grinding wheel. The thermocouple position, workpiece feed direction, wheel rotation, and load cell used for force measurement are indicated. Schematic only, scale and geometry not represented.

$$Ec = \frac{F_t.v_s}{Q_w} \quad (2)$$

where F_t is the tangential grinding force (N), v_s is the cutting speed (m/s), and Q_w is the material removal rate (mm^3/s).

The grinding parameters used in the tests are summarized in Table 2. All experiments were conducted with a constant wheel speed of 5000 rpm and a workpiece feed rate of 100 mm/min, in up-grinding mode. Six depths of cut (a_e = 10, 20, 50, 80, 100, and 120 μm) were evaluated. Before the grinding tests, each wheel was carefully mounted and aligned with the spindle axis to ensure concentric positioning, followed by dressing with a multi-point diamond tool. The assembled system was then operated at 5000 rpm for verification, during which no abnormal vibration or noise was observed. This confirmed that the wheel–spindle assembly was properly centered and dynamically stable under the test conditions.

After each grinding test, the ground surfaces were visually inspected under white light illumination. No signs of thermal damage or grinding burn (e.g., discoloration or oxidation marks) were observed, indicating that the process remained thermally stable under all test conditions.

Distilled water was used as the cutting fluid for both lubrication strategies, applied at a constant flow rate of 400 mL/min. This ensured a stable and reproducible test environment, minimizing the influence of additives and preventing contamination of the internal cooling system.

Each condition was tested in triplicate, and the mean values were used for comparative analysis.

Results and discussion

The results and discussion are structured in two main parts. The first focuses on the dynamic evolution of grinding forces and temperature along the grinding pass, allowing the identification of distinct thermal zones. In this part, the three-layer structured wheel is presented as a representative case of internal cooling and compared with the conventional wheel under external flooding. The second part analyzes the overall tribological and thermal performance based on average values of tangential and normal forces, force ratio, specific energy and temperature variation (ΔT), where both the one-layer and three-layer wheels are directly compared to the conventional configuration across different cutting depths.

This dual approach provides both a localized view of thermal behavior and a macroscopic evaluation of process efficiency, enabling a comprehensive assessment of how internal cooling with radial channels enhances grinding performance.

Table 2
Grinding parameters used in the tests for evaluating external and internal cooling systems.

Grinding process parameters	Values
Grinding wheel speed V_S	16.23 m/s
Workpiece feed rate V_W	100 (mm/min)
Depth of cut, a_e	10, 20, 50, 80, 100, 120 (μm)
Fluid flow rate	400 ml/min – distilled water
Grinding mode	Up Grinding
Grinding wheel abrasive	Alumina (Ø 62 × 15 × 21 mm)
Workpiece	AISI 1045 (80 × 15 × 10 mm); 198 HV

3.1. Identification of cutting stages

The concept of the three cutting stages in grinding was originally proposed by Malkin and Guo (2007) [56] to describe the evolution of abrasive interaction between the grinding wheel and the workpiece over time. This approach, widely recognized in the literature, is used in the present work as the basis for thermal and force analysis. Fig. 8a presents a schematic representation of the three grinding stages, namely cut-in, steady state, and cut-out, under conventional flood lubrication. In this case, fluid penetration into the contact zone can be hindered by the air barrier formed by the rotating wheel, leading to a delayed cooling effect and higher temperature gradients. Fig. 8b illustrates the corresponding stages for structured wheels with internal cooling. In this configuration, coolant is supplied directly to the contact zone through the internal channels, which conceptually allows more immediate fluid availability at cut-in, continuous delivery during steady-state, and improved cooling conditions at cut-out. This schematic highlights the expected differences in thermal distribution and contact dynamics between internal cooling and traditional external flooding.

Fig. 9 shows the profile of the tangential force (*Ft*) experimentally obtained in this study for a depth of cut of 120 μm, under both cooling systems. The three stages described by Malkin and Guo (2007) [56] are clearly observable:

- Cut in (0 – ~4 mm): initial contact between the grinding wheel and the workpiece. Forces increase until the effective depth of cut is established.
- Steady state (~4 – ~12.5 mm): constant material removal with stabilized forces.
- Cut out (~12.5 – ~15 mm): final stage, where the grinding wheel gradually leaves the workpiece. The contact area decreases, which leads to a progressive reduction in forces.

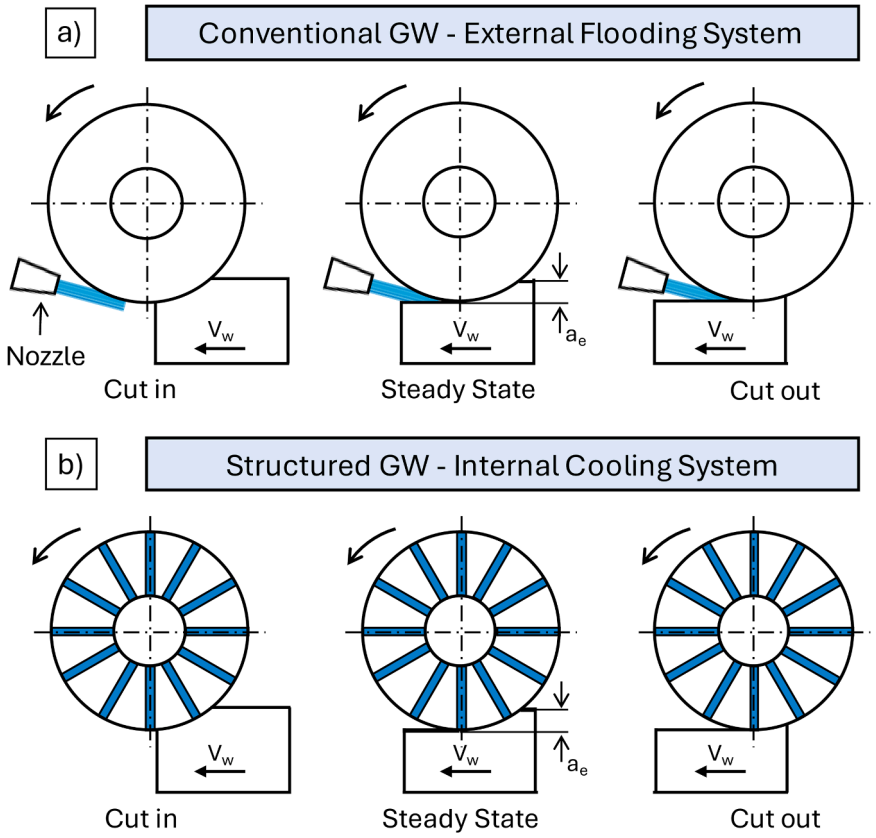

Fig. 8. Schematic representation of the three grinding stages — cut in, steady state, and cut out — for a conventional flood lubrication system (a) and a structured grinding wheel with internal cooling (b). Adapted from Malkin and Guo (2007) [27]. Schematic only, scale and geometry not represented.

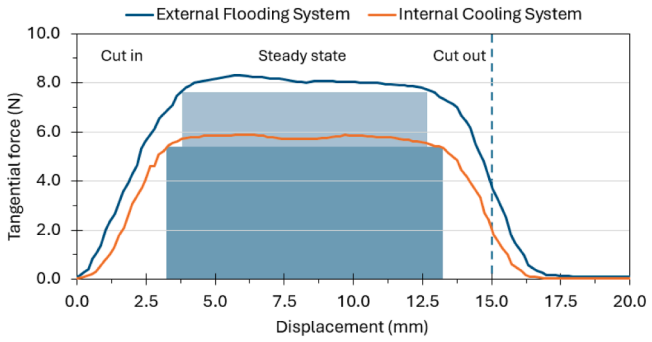

Fig. 9. Tangential force profile during the grinding operation for conventional and structured wheels, with the three stages identified from the force signal.

It is noticeable that with the internal cooling system the steady-state regime is more quickly reached with a lower tangential force intensity, indicating an earlier and more efficient stabilization of the process.

Furthermore, the average force value during the steady-state is visibly lower for the system with internal channels, highlighting the tribological improvement associated with the direct fluid delivery to the cutting arc.

In addition to mechanical signals, the thermal behavior of the workpiece was examined to better understand the fluid action in each grinding stage. Fig. 10 presents the temperature profiles measured by thermocouples and the heating rates of the workpiece for two cutting depth conditions (lower and highest): 10 μm (Figs. 10a and 10b) and 120 μm (Figs. 10c and 10d). The interpretation of the thermal data was based on three thermal zones (Z1, Z2, Z3), defined according to the variations in the heating rate observed in the graphs.

The analysis of the data from Fig. 10 allows the identification of three distinct thermal zones along the grinding path. Zone Z1 (0–5 mm) corresponds to the initial heating of the workpiece and matches the cut-in phase. In this region, the grinding wheel is approaching the thermocouple position (located at 7.5 mm), and the temperature rise is primarily attributed to lateral thermal conduction. At this stage, heat generation is still limited, and therefore no significant differences are observed between the two lubrication systems.

Z2 (5 – 10 mm) represents the thermal steady-state regime, in which the grinding wheel fully covers the thermocouple region. It is in this region that the most significant effect of internal cooling is observed: for $a_e = 10$ μm, the heating rate was 78 % lower compared to the conventional system; for $a_e = 120$ μm, the reduction was 52 %. This difference reflects the direct action of the cooling channels, which deliver the fluid directly to the cutting arc from the beginning of contact through to the exit, as illustrated in Fig. 7b

In the conventional system, Fig. 8a, the fluid is sprayed behind of the active zone, but its entry to the contact zone is partially hindered by the air layer generated by the wheel rotation, a phenomenon well described by Mihic et al. (2013) [57], who highlight how this aerodynamic barrier reduces the effective fluid flow reaching the abrasive interface. With internal cooling, the channels overcome this limitation, taking the fluid directly to the cutting zone, increasing the thermal efficiency of the process and reducing the heating rate of the part.

Z3 (10 – ~12.5 mm) corresponds to the region where the temperature peak occurs. Although this interval is close to the cut-out phase of the grinding wheel, its definition here is based on the point of maximum measured temperature rather than the complete disengagement of the wheel from the workpiece (which occurs at 15 mm). The delimitation up to the peak is necessary to analyze the heating rate, since after this point, the workpiece begins to cool down.

Within this region, the temperature rises more significantly in both

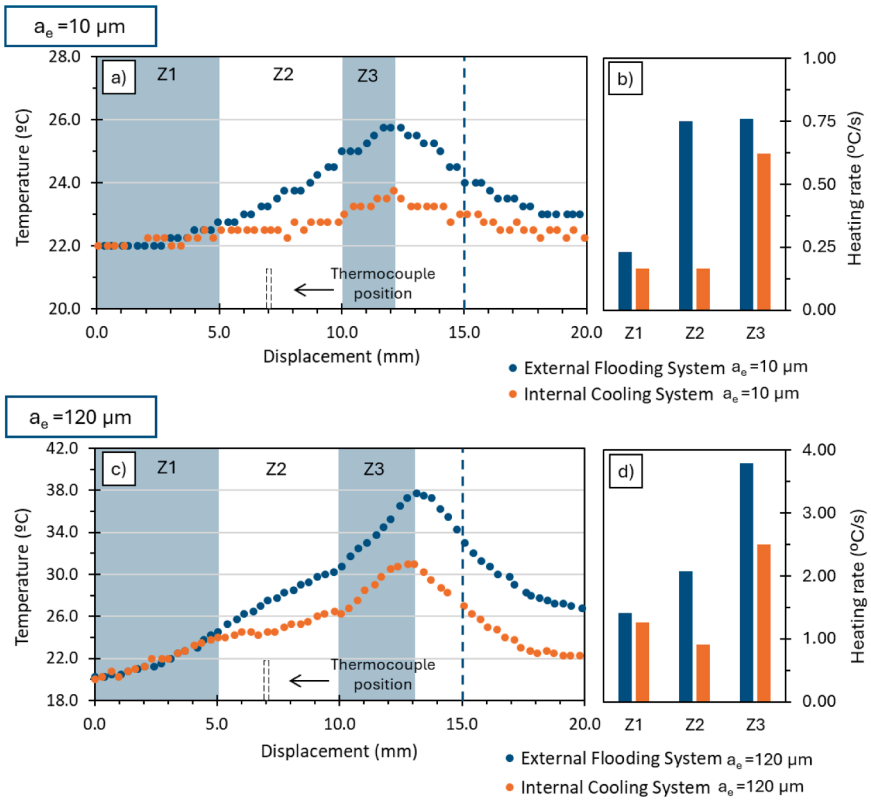

Fig. 10. Temperature profiles measured by thermocouple for cutting depths of 10 µm (a) and 120 µm (c), and corresponding heating rates (b, d), for both lubrication systems. The thermocouple was positioned 7.5 mm from the start of the grinding path, as shown in (a) and (c), and 1 mm below the surface.

systems. The thermal peak occurs after the grinding wheel passes the thermocouple (positioned at 7.5 mm), which can be explained by two main factors. First, as reported by Malkin and Guo (2007) [56], during the final stage of the grinding pass (cut-out stage), there is a sudden reduction in the workpiece's ability to conduct heat, since less material remains beneath the active zone of the grinding wheel, as shown in Fig. 8. As a result, part of the heat that was previously conducted into the interior of the workpiece begins to accumulate at the surface, leading to a localized temperature increase. In addition, it is important to consider that throughout the grinding pass, part of the generated heat is removed along with the chips. However, during the final stage (cut-out), chip generation progressively decreases, and this heat removal mechanism is also reduced. This condition, combined with the reduced mass of the workpiece beneath the cutting zone, contributes to thermal accumulation in the exit region.

It was also observed that the temperature peaks in the tests with $a_e =$ 10 µm occurred slightly earlier than those observed in $a_e = 120$ µm. This anticipation may be associated with the lower heat generation under milder cutting conditions, which reduces thermal accumulation along the grinding pass and causes the temperature peak to be reached earlier.

For $a_e = 10$ µm, the data show that in the conventional system, the heating rate always remains high between Z2 and Z3, while in the system with internal channels, a significant increase is observed when moving to the last zone. Nevertheless, the heating rate in Z3 is still 18.2 % lower than that of the conventional system. This behavior reinforces that the internal fluid delivery was highly effective in containing the thermal rise during the steady-state cutting phase (Z2). Although this gain decreases in Z3, the maximum temperature reached remains significantly lower than in the conventional condition, demonstrating that the earlier thermal control was decisive in limiting the final temperature (highest temperature in each zone during grinding).

With a $a_e = 120$ µm, the decrease in heating rate in Z3 was 33.9 %, suggesting that the internal channel system kept better performance than the conventional system even under more hostile conditions.

These findings reinforce the value of thermal segmentation into three distinct zones, which enabled a more precise analysis of the workpiece heating evolution throughout the grinding pass. While Zone Z1 showed similar behavior across all configurations, significant differences emerged in Z2 and Z3. The reduction in heating rate was primarily driven by the action of the internal channels during Z2, where fluid delivery was more efficient. This earlier thermal control contributed to lower peak temperatures in Z3, even when the heating rate increased, confirming the importance of continuous and localized cooling.

Moreover, the structured wheels, especially the three-layer configuration, proved effective in minimizing thermal accumulation throughout the entire grinding path. The combination of internal cooling and zone-based analysis offered a detailed understanding of how fluid delivery influences the thermal response of the system.

This three-zone segmentation, integrated with the classical cutting stages, provides a robust framework to interpret both thermal and mechanical phenomena during grinding. It facilitates a more accurate assessment of coolant efficiency and material behavior, particularly under transient and high-load conditions.

3.2. *Overall performance of the structured grinding wheels*

This section consolidates the average results obtained from the grinding tests, focusing on key performance indicators: tangential force, normal force, specific grinding energy, force ratio, and temperature variation (ΔT). The data were evaluated across different depths of cut and wheel configurations, enabling a direct comparison between the conventional reference wheel (external flooding) and the structured wheels incorporating one or three layers of internal channels. This comparative analysis aims to assess how internal cooling affects both mechanical and thermal loads, providing insights into the process efficiency and the effectiveness of localized fluid delivery during grinding.

Fig. 11 presents the average values of tangential force (11a) and normal force (11b) in the steady-state regime as a function of the depth of cut, comparing three conditions: a Reference grinding wheel without channels and with conventional external flooding, and two structured wheels with internal cooling, containing one and three layers of radial channels (Table 1).

In all analyzed conditions, the presence of channels promoted a significant reduction in grinding forces, with the three-layer wheel showing the lowest absolute values. At lower depths of cut ($a_e = 10$ μm), the tangential force was reduced by 49.3 % with three layers and by 33.2 % with one layer. At the maximum depth of cut ($a_e = 120$ μm), the reductions were 31.3 % and 12.6 %, respectively. A similar reduction was also observed for the normal force, with reductions of up to 37.6 % (three layers) and 28.4 % (one layer), for 120 μm.

Furthermore, it is observed that with the increase in depth of cut, the effectiveness of the wheel with one layer tends to decrease, resulting in smaller force reductions compared to the low-penetration condition. On the other hand, the three-layer wheel shows stable performance even under more extreme cutting conditions, as it maintains a constant force reduction throughout the range studied. This behavior emphasizes the benefit of fluid dispersion at various levels of the wheel width, thus ensuring a more efficient action along the entire contact arc.

Fig. 12 shows the force ratio as a function of depth of cut for the three grinding wheel configurations. The reference wheel with external cooling maintained nearly constant values around 0.77 across the entire range, indicating high and persistent frictional interaction. In contrast, the structured wheels exhibited a lower force ratio at low-to-moderate depths of cut, with a gradual increase at higher cuts.

The three-layer wheel consistently presented the lowest force ratio values. At 10 μm, for instance, its force ratio was 21.3 % lower than that of the reference. This behavior highlights the improved lubrication conditions provided by direct fluid delivery, especially in shallow grinding conditions where the contact zone is narrower and more sensitive to fluid efficiency. The one-layer wheel also showed improvements, but with less intensity.

As the depth of cut increased, the force ratio values among the wheels tended to converge. This convergence suggests a partial saturation of the fluid's lubricating action, possibly caused by elevated heat generation and an expanded contact area, which intensify material-wheel interactions. Even so, the structured wheels, particularly the three-layer design, maintained a tribological advantage across nearly all depths tested.

These trends align with the observed reductions in specific grinding energy (Fig. 13), a key indicator of process efficiency. Both structured wheels demonstrated significantly lower energy requirements compared to the conventional wheel, especially at 10–50 μm. The three-layer wheel achieved energy savings of up to 50 %, confirming its superior ability to reduce friction and dissipate heat effectively.

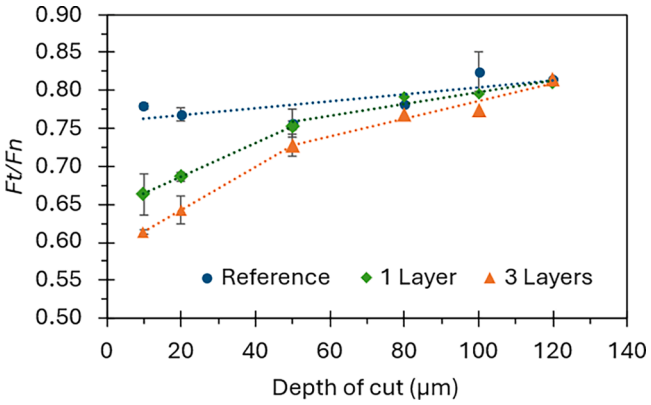

Fig. 12. Force Ratio (Ft/Fn) as a function of depth of cut for the Reference wheel (external flooding) and structured wheels with one and three internal coolant layers (internal cooling).

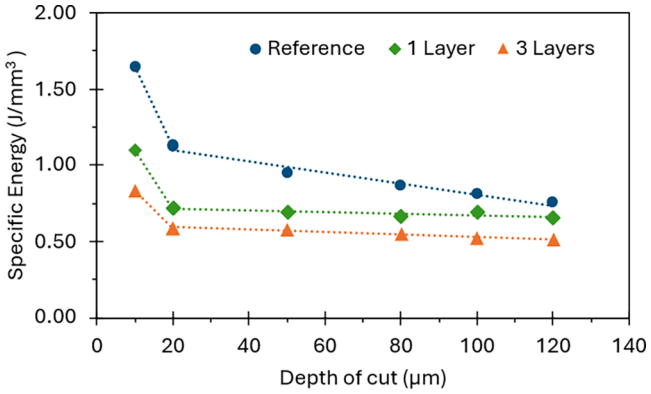

Fig. 13. Specific grinding energy as a function of depth of cut for the reference wheel (external flooding) and structured wheels with one and three internal coolant layers (internal cooling).

It is worth noting that, despite lower grinding forces, the specific energy at 10 μm was the highest among all conditions. This occurs because energy per unit volume is inversely proportional to the material removal rate. At such a shallow depth of cut, the amount of removed material is minimal, which amplifies the energy value even under favorable tribological conditions. In other words, less material is removed for the same amount of input energy, resulting in a higher specific energy value.

In addition, at these shallow depths, the abrasive grains may interact

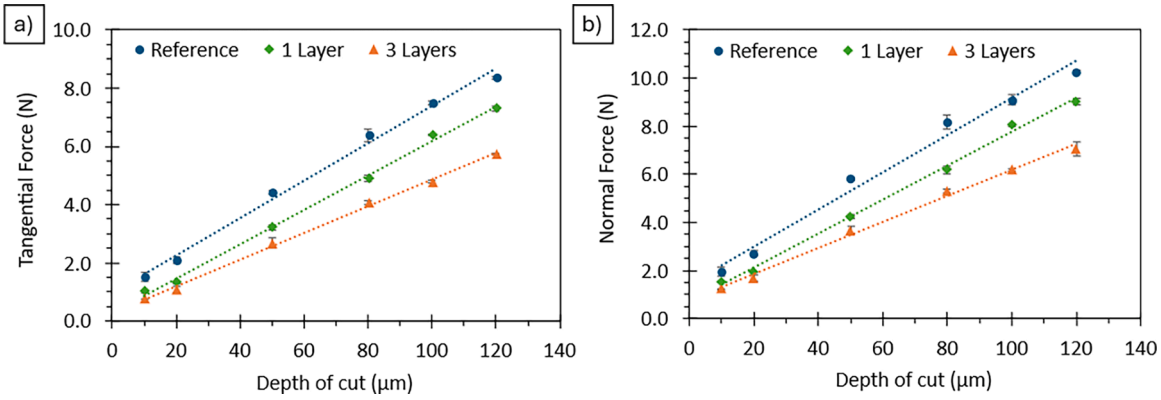

Fig. 11. Tangential (a) and normal (b) grinding forces as a function of depth of cut for the reference wheel (external flooding) and structured wheels with one and three internal coolant layers (internal cooling).

primarily through sliding and elastic-plastic deformation rather than effective cutting. This "plowing" mechanism contributes to energy consumption without substantial material removal, further increasing the specific energy despite the low force levels [58].

This correlation between lower force ratio and reduced energy consumption demonstrates how enhanced fluid accessibility not only improves lubrication but also contributes to a more efficient energy transfer during material removal. In contrast, the reference wheel exhibited higher energy demands, consistent with its higher force ratio and limited cooling efficiency.

At higher depths (80–120 μm), all wheels showed an increase in specific energy, with a diminishing gap between them. This behavior suggests that, under severe cutting conditions, the current channel design and the tested cooling fluid flow rate approaches its hydraulic and thermal limits. Nonetheless, even at 120 μm, the three-layer wheel still delivered measurable benefits compared to the conventional system.

The lower tangential force and reduced specific energy observed with internal cooling suggest a more efficient cutting regime, which is typically associated with reduced grain flattening and bond smearing, and a greater tendency for micro-fracture rather than severe attrition. This indicates that the multilayer channel design not only improves cooling but may also mitigate adverse tribological wear processes.

Fig. 14 presents the average temperature variation (ΔT) recorded during the tests, defined as the difference between the initial temperature and the thermal peak at each depth of cut. The repeatability of the measurements was also verified, and the maximum standard deviation was ±0.65 °C.

In all tested conditions, the Reference wheel exhibited the highest ΔT values. The introduction of internal cooling resulted in significant reductions in thermal variation, especially at lower depths of cut, where the channel system was more effective in limiting heat accumulation in the contact zone. At these lower depths, thermal variation was also smaller, indicating a more stable and controlled thermal environment, the most favorable condition for avoiding thermal damage during grinding.

With 3 channel layers, the ΔT reduction reached 58.6 % at 10 μm and 51.6 % at 20 μm, and was still 35.4 % at the highest depth of cut (120 μm). In contrast, with a single layer, the gains were more modest but still consistent, with reductions of 17.2 % at $a_e = 10$ μm and 24.8 % at $a_e = 120$ μm.

These results demonstrate that even with the same fluid volume, the precise distribution provided by the multi-layer internal channels is crucial for thermal performance. The three-layer structured wheel promoted a more uniform and continuous fluid distribution in the active zone, enabling more effective dissipation of the heat generated during grinding. Furthermore, in the experimental setup used, the cooling fluid is continuously dispensed along the entire perimeter. Assuming a useful cooling zone (contact zone) of ~60° [48] the actual cooling fluid volume used will be ~70 mL/min.

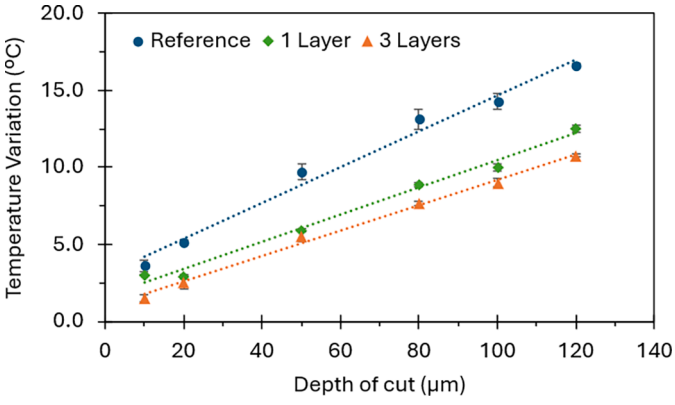

Fig. 14. Maximum temperature variation (ΔT) measured by thermocouple as a function of depth of cut for the reference wheel (external flooding) and structured wheels with one and three internal coolant layers (internal cooling).

The superior performance of the three-layer configuration can be further explained by its enhanced fluid dynamics. A complementary CFD study conducted by the same research group [54] showed that this configuration enables a more uniform and dynamic fluid distribution along the contact zone, effectively minimizing dry regions and improving cooling efficiency throughout the grinding cycle. Unlike the single-layer design, which concentrates fluid delivery at a fixed radial level, the multilayer topology ensures continuous replenishment of coolant across the wheel width. This behavior contributes to reducing thermal gradients, stabilizing grinding forces, and improving energy efficiency, corroborating the experimental findings presented in this work.

At a depth of cut of 120 μm, the three-layer configuration achieved a ΔT of approximately 10 °C, which is comparable to the ΔT of the reference wheel at only 50 μm (~11 °C). This means that more than double the depth of material could be removed without increasing the thermal load.

Overall, the introduction of internal channels had a positive impact across all evaluated variables. The three-layer wheel not only delivered the best results in terms of thermal control and force reduction but also maintained stable behavior even at higher material removal rates, confirming its robustness for industrial applications.

These findings reinforce the potential of multi-layer structured wheels as a high-performance solution for internal cooling. By enabling higher depths of cut without raising temperatures or increasing fluid consumption, this approach contributes directly to productivity gains, improved process stability, and sustainability goals through more efficient fluid use.

No clogging of the internal channels was observed during the tests. This can be attributed to the relatively large channel diameter (1.7 mm) compared with the chip size, which is of the same order as the abrasive grain size (220 mesh). The use of distilled water also minimized the presence of external particles that could obstruct the flow, further reducing the likelihood of blockage. From an industrial perspective, the method remains attractive due to its compatibility with conventional pressing–sintering routes and the low cost of sacrificial polymer inserts, which makes large-scale application feasible. Moreover, despite the introduction of multiple channels, no signs of cracking or mechanical instability were detected during testing, confirming that the proposed design preserved a sufficient wheel structural integrity for grinding under different operation conditions.

Conclusions

This study evaluated the performance of three-dimensionally structured vitrified grinding wheels specifically designed for internal cooling and compared them to a conventional wheel operating under external flood cooling.

- Thermal response: Internal cooling proved highly effective in stabilizing workpiece temperature. During the steady-state grinding phase, heating rates were reduced by up to 78 % at 10 μm, and 52 % at 120 μm, confirming that direct fluid delivery through internal channels enables more efficient and uniform heat removal along the grinding path.
- Mechanical efficiency: Tangential and normal forces were significantly lowered. The three-layer wheel reduced tangential force by up to 49.3 % and normal force by 37.6 %, highlighting the benefit of multi-depth fluid access across the wheel width.
- Tribological performance: The force ratio decreased by up to 21.3 %, particularly at low depths, demonstrating enhanced lubrication and reduced friction from internal cooling.

- Thermal stability (ΔT): The three-layer wheel achieved ΔT reductions of 58.6 % at $a_e = 10$ μm and 35.4 % at $a_e = 120$ μm. Notably, the temperature at $a_e = 120$ μm was comparable to the conventional system at $a_e = 50$ μm, enabling more than double the material removal without thermal overload.
- Comparative performance: The three-layer configuration outperformed the single-layer design by achieving 21 % greater force reduction and 41 % greater ΔT reduction on average, underscoring the importance of channel distribution along the contact arc.

Overall, the results confirm that structured grinding wheels with multi-layer internal channels offer a robust and scalable solution to enhance grinding performance. They enable higher cutting depths and thermal stability without increasing coolant consumption, aligning with current demands for productivity and sustainable manufacturing.

The innovative fabrication method using sacrificial 3D-printed structures proved effective and reproducible, allowing for the integration of multilayered channels within a monolithic vitrified matrix, a step forward in the design of smart, self-cooling abrasive tools.

CRediT authorship contribution statement

Sharlane Costa: Writing – review & editing, Writing – original draft, Methodology, Investigation, Formal analysis, Conceptualization. **Paulina Capela:** Writing – review & editing. **Amauri Hassui:** Writing – review & editing, Resources, Methodology. **João Ribeiro:** Writing – review & editing, Supervision, Software, Resources, Formal analysis, Data curation. **Mário Pereira:** Writing – review & editing, Supervision, Resources, Investigation, Data curation. **Delfim Soares:** Writing – review & editing, Validation, Supervision, Resources, Project administration, Methodology, Investigation, Formal analysis, Conceptualization.

Declaration of competing interest

The authors of this work declare that there is no conflict of interest.

Acknowledgements

This work was supported by FCT national funds, under the national support to R&D units grant, through the reference project UIDB/04436. The authors are grateful to the Foundation for Science and Technology (FCT, Portugal) for financial support through national funds FCT/MCTES (PIDDAC) to CIMO (UIDB/00690/2020 and UIDP/00690/2020) and SusTEC (LA/P/0007/2020). This work is within the scope of Sharlane Costa Ph.D. degree, in progress, financially supported by the Portuguese Foundation for Science and Technology (FCT) through the Ph.D grant reference 2021.07352.BD (DOI:https://doi.org/10.54499/2021.07352.BD). Paulina Capela acknowledges the financial support from FCT through the doctoral grant 2024.01273.BDANA.

Data availability

No data was used for the research described in the article.

References

[1] X. Fu, L. Lv, B. Chen, Z. Deng, M. Wu, Pre-control of grinding surface quality by data-driven: a review, Int. J. Adv. Manuf. Technol. 133 (2024) 3081–3104, https://doi.org/10.1007/s00170-024-13921-0.
[2] H.N. Li, T.B. Yu, Z.X. Wang, L. Zhu, W.A.W.S. Da, Detailed modeling of cutting forces in grinding process considering variable stages of grain-workpiece micro interactions, Int. J. Mech. Sci. 126 (2017) 319–339, https://doi.org/10.1016/J.IJMECSCI.2016.11.016.
[3] C. Heinzel, B. Kirsch, D. Meyer, J. Webster, Interactions of grinding tool and supplied fluid, CIRP Ann. 69 (2020) 624–645, https://doi.org/10.1016/J.CIRP.2020.05.001.
[4] Z. Crowson, J. Billingham, P. Houston, Lubrication flow in grinding, J. Eng. Math. 147 (2024) 12, https://doi.org/10.1007/s10665-024-10383-x.
[5] J.E. Manikanta, N. Ambhore, C. Nikhare, Application of sustainable techniques in grinding process for enhanced machinability: a review, J. Braz. Soc. Mech. Sci. Eng. 46 (2024) 199, https://doi.org/10.1007/s40430-024-04801-5.
[6] B.K. Sato, J.C. Lopes, R.L. Rodriguez, M.V. Garcia, F.S.F. Ribeiro, P.R. Aguiar, et al., Eco-friendly manufacturing towards the industry of the future with a focus on less cutting fluid and high workpiece quality applied to the grinding process, Int. J. Adv. Manuf. Technol. 113 (2021) 1163–1172, https://doi.org/10.1007/s00170-021-06650-1.
[7] E. Brinksmeier, C. Heinzel, W.I.M. Friction, Cooling and lubrication in grinding, CIRP Ann. 48 (1999) 581–598, https://doi.org/10.1016/S0007-8506(07)63236-3.
[8] R. Peng, L. Zhao, J. Tong, M. Chen, M. Zhou, A. Li, Design and evaluation of an internal-cooling grooved grinding wheel, J. Manuf. Process. 73 (2022) 1–16, https://doi.org/10.1016/J.JMAPRO.2021.10.061.
[9] Jayakumar K. Effect of grinding parameters and coolants on grindability of Ti grade 9 alloy. Mater Today Proc 2024. https://doi.org/10.1016/j.matpr.2024.04.030.
[10] M. Hadad, B. Sadeghi, Minimum quantity lubrication-MQL turning of AISI 4140 steel alloy, J. Clean. Prod. 54 (2013) 332–343, https://doi.org/10.1016/J.JCLEPRO.2013.05.011.
[11] A. Basem, M. Naji, H.A. Al-Asadi, M. Sediq Safi, G. Daminova, M. Alhadrawi, et al., Small-quantity cooling lubrication in creep-feed grinding: surface quality and residual stress analysis, Results. Eng. 22 (2024) 102348, https://doi.org/10.1016/j.rineng.2024.102348.
[12] A. Elsheikh, A.B.M. Ali, A. Saba, H. Faqeha, A.A. Alsaati, A.M. Maghfuri, et al., A review on sustainable machining: technological advancements, health and safety considerations, and related environmental impacts, Results. Eng. 24 (2024) 103042, https://doi.org/10.1016/J.RINENG.2024.103042.
[13] Y. Zhang, L. Li, X. Cui, Q. An, P. Xu, W. Wang, et al., Lubricant activity enhanced technologies for sustainable machining: mechanisms and processability, Chin. J. Aeronaut. 38 (2025) 103203, https://doi.org/10.1016/j.cja.2024.08.034.
[14] K.C. Wickramasinghe, H. Sasahara, E.A. Rahim, G.I.P. Perera, Green Metalworking Fluids for sustainable machining applications: a review, J. Clean. Prod. 257 (2020) 120552, https://doi.org/10.1016/J.JCLEPRO.2020.120552.
[15] K. Kishore, S.R. Chauhan, M.K. Sinha, Application of machine learning techniques in environmentally benign surface grinding of Inconel 625, Tribol. Int. 188 (2023) 108812, https://doi.org/10.1016/J.TRIBOINT.2023.108812.
[16] D. Li, T. Zhang, T. Zheng, N. Zhao, Z. Li, A comprehensive review of minimum quantity lubrication (MQL) machining technology and cutting performance, Int. J. Adv. Manuf. Technol. 133 (2024) 2681–2707, https://doi.org/10.1007/s00170-024-13902-3.
[17] M. Iruj, S. Yaqoob, J.A. Ghani, H. Jaber, N. Saibani, M. Alkhedher, State-of-the-art hybrid lubrication (Cryo-MQL) supply systems, performance evaluation, and optimization studies in various machining processes, Results. Eng. 22 (2024) 102090, https://doi.org/10.1016/J.RINENG.2024.102090.
[18] S.H. Musavi, M. Razfar, D.D. Ganji, New application of ionic liquid as a green-efficient lubricant, Results. Eng. 21 (2024) 101773, https://doi.org/10.1016/J.RINENG.2024.101773.
[19] A. Sharma, A. Chaudhari, M.Z.K. Yusufzai, M. Vashista, Effectiveness of using liquid nitrogen cryogen in grinding to enhance the grinding performance of hard steel, Proc. Inst. Mech. Eng. B J. Eng. Manuf. 238 (2024) 315–327, https://doi.org/10.1177/09544054221147622.
[20] H.N. Li, K.G. Xie, B. Wu, W.Q. Zhu, Generation of textured diamond abrasive tools by continuous-wave CO2 laser: laser parameter effects and optimisation, J. Mater. Process. Technol. 275 (2020) 116279, https://doi.org/10.1016/J.JMATPROTEC.2019.116279.
[21] S. Fang, F. Soldera, A. Rosenkranz, T. Herrmann, D. Bähre, L. Llanes, et al., Microstructural and metallurgical assessment of the laser-patterned cemented tungsten carbide (WC-CoNi), Procedia Manuf. 26 (2018) 198–204, https://doi.org/10.1016/j.promfg.2018.07.027.
[22] X. Zhao, T. Yu, C. Jia, S. Lu, L. Chen, W. Wang, Study on textured CBN grinding wheel by laser cladding, Int. J. Adv. Manuf. Technol. 106 (2020) 865–876, https://doi.org/10.1007/s00170-019-04240-w.
[23] B. Kirsch, The impact of contact zone flow rate and bulk cooling on the cooling efficiency in grinding applying different nozzle designs and grinding wheel textures, CIRP. J. Manuf. Sci. Technol. 18 (2017) 179–187, https://doi.org/10.1016/J.CIRPJ.2017.02.002.
[24] H.N. Li, Y.J. Zhao, S. Cao, H. Chen, C. Wu, H. Qi, et al., Controllable generation of 3D textured abrasive tools via multiple-pass laser ablation, J. Mater. Process. Technol. 295 (2021) 117149, https://doi.org/10.1016/J.JMATPROTEC.2021.117149.
[25] A. Bhowmik, B. Sen, N. Beemkumar, J. Singh Chohan, P.S. Bains, G. Singh, et al., Development and wear resistivity performance of SiC and TiB2 particles reinforced novel aluminium matrix composites, Results. Eng. 24 (2024) 102981, https://doi.org/10.1016/J.RINENG.2024.102981.
[26] J. Ma, E. Cui, B. Zha, G. Zheng, K. Li, X. Cheng, et al., Experimental assessment of cryogenic LN2 enhanced GNPs-Cu/ZrO2 multiphase composite nano-fluids MQL in the turning of GH4169, Mater. Today Commun. 48 (2025) 113321, https://doi.org/10.1016/J.MTCOMM.2025.113321.
[27] T. He, N. Liu, H. Xia, L. Wu, Y. Zhang, D. Li, et al., Progress and trend of minimum quantity lubrication (MQL): a comprehensive review, J. Clean. Prod. 386 (2023) 135809, https://doi.org/10.1016/J.JCLEPRO.2022.135809.
[28] E. Benedicto, D. Carou, E.M. Rubio, Technical, economic and environmental review of the lubrication/cooling systems used in machining processes, Procedia Eng. 184 (2017) 99–116, https://doi.org/10.1016/J.PROENG.2017.04.075.

[29] A.M. Khan, S. Anwar, M. Jamil, M.M. Nasr, M.K. Gupta, M. Saleh, et al., Energy, environmental, economic, and technological analysis of Al-GnP nanofluid- and cryogenic LN2-assisted sustainable machining of Ti-6Al-4V alloy, Met 2021 11 (2021) 88, https://doi.org/10.3390/MET11010088, 11, Page 88.
[30] H.N. Li, D. Axinte, Textured grinding wheels: a review, Int. J. Mach. Tools. Manuf. 109 (2016) 8–35, https://doi.org/10.1016/J.IJMACHTOOLS.2016.07.001.
[31] S. Zhang, Z. Zhang, H. Xing, G. Hao, X. Liang, Analysis and optimization of abrasive waterjet dressing parameters for surface texturing of diamond grinding wheels, Diam. Relat. Mater. 149 (2024) 111661, https://doi.org/10.1016/J.DIAMOND.2024.111661.
[32] M. Barmouz, B. Azarhoushang, Additive manufacturing of hybrid bond grinding wheels via digital light processing: performance enhancement through composition alteration and groove incorporation, Results. Eng. 27 (2025) 105808, https://doi.org/10.1016/J.RINENG.2025.105808.
[33] K.G. Xie, A.G.A. Rushworth, H. Chen, J. Li, On the modelling and experimental study of CO2 laser ablation on resin-bond diamond grinding wheels: understanding the effect of processing parameters on the time-dependent temperature field, J. Manuf. Process. 124 (2024) 1471–1484, https://doi.org/10.1016/J.JMAPRO.2024.07.007.
[34] S.B. Thekkoot Surendran, V. Sooraj, Sweating type surface grinding wheels for self-adaptable lubricant delivery governed by cutting temperature and speed, J. Manuf. Process. 134 (2025) 915–931, https://doi.org/10.1016/J.JMAPRO.2024.12.081.
[35] S. Costa, M. Pereira, J. Ribeiro, D. Soares, Texturing methods of abrasive grinding wheels: a systematic review, Materials 15 (2022) 8044, https://doi.org/10.3390/ma15228044.
[36] R. Peng, J. Tong, X. Tang, X. Huang, K. Liu, Application of a pressurized internal cooling method in grinding inconel 718: modeling-simulation and testing-validation, Int. J. Mech. Sci. 189 (2021) 105985, https://doi.org/10.1016/J.IJMECSCI.2020.105985.
[37] M. Chen, R. Peng, A. Li, X. Xiao, L. Zhao, Assessment of surface structure optimization in internal cooling grinding, Int. J. Adv. Manuf. Technol. 123 (2022) 2139, https://doi.org/10.1007/s00170-022-10304-1, 55.
[38] L. Zhao, R. Peng, J. Gao, Y. Li, M. Chen, Mechanistic design of porous self-lubricating grinding wheels with integrated internal cooling: role of PMMA and nickel-coated MoS_2 composites in machining enhancement, J. Mater. Process. Technol. 340 (2025) 118877, https://doi.org/10.1016/J.JMATPROTEC.2025.118877.
[39] R. Peng, Y. Luo, B. Liu, J. Tong, L. Zhao, Application of bionic phyllotaxis in internal cooling cup wheel: modeling-simulation and experimental verification, Int. J. Adv. Manuf. Technol. 114 (2021) 3803–3822, https://doi.org/10.1007/s00170-021-07097-0.
[40] R. Peng, K. Liu, J. Tong, X. Tang, Performance of the internal-cooling grooved grinding wheel with patterned abrasives, Int. J. Adv. Manuf. Technol. 106 (2020) 1633–1644, https://doi.org/10.1007/s00170-019-04694-y.
[41] M. Li, W. Wang, Y. Huang, S. Yan, P. Zhang, L. Zou, 3D printed compliance tool incorporated internal-impeller structure for high performance face grinding of titanium alloy, J. Mater. Process. Technol. 329 (2024) 118446, https://doi.org/10.1016/J.JMATPROTEC.2024.118446.
[42] G. Guerrini, F. Lerra, A. Fortunato, The effect of radial infeed on surface integrity in dry generating gear grinding for industrial production of automotive transmission gears, J. Manuf. Process. 45 (2019) 234–241, https://doi.org/10.1016/J.JMAPRO.2019.07.006.
[43] A.Z.B. Abrasives. Tribology and fundamentals of abrasive machining Processes: third Edition 2021:3–30. https://doi.org/10.1016/B978-0-12-823777-9.00009-4.
[44] Y. Qiu, B. Zhao, Y. Cao, W. Ding, Y. Fu, C. Pu, On the grinding performance of alumina wheels in ultrasonic vibration–assisted grinding of hardened GCr15 steel, Int. J. Adv. Manuf. Technol. 120 (2022) 1695–1706, https://doi.org/10.1007/s00170-022-08894-x.
[45] Q. Miao, W. Ding, W. Kuang, J. Xu, Tool wear behavior of vitrified microcrystalline alumina wheels in creep feed profile grinding of turbine blade root of single crystal nickel-based superalloy, Tribol. Int. 145 (2020) 106144, https://doi.org/10.1016/J.TRIBOINT.2019.106144.
[46] M. Barmouz, B. Azarhoushang, Grinding performance evaluation of additively manufactured vitrified bond Grinding wheel: tool wear, Grinding force, surface roughness, and surface topography analysis, Int. J. Precis. Eng. Manuf.-Green Technol. (2025) 1, https://doi.org/10.1007/s40684-024-00684-y, 16.
[47] K. Nadolny, Small-dimensional sandwich grinding wheels with a centrifugal coolant provision system for traverse internal cylindrical grinding of steel 100Cr6, J. Clean. Prod. 93 (2015) 354, https://doi.org/10.1016/J.JCLEPRO.2015.01.046, 63.
[48] J. Sieniawski, K. Nadolny, The effect upon grinding fluid demand and workpiece quality when an innovative zonal centrifugal provision method is implemented in the surface grinding of steel CrV12, J. Clean. Prod. 113 (2016) 960, https://doi.org/10.1016/J.JCLEPRO.2015.11.017, 72.
[49] T. Nguyen, L.C. Zhang, Performance of a new segmented grinding wheel system, Int. J. Mach. Tools. Manuf. 49 (2009) 291, https://doi.org/10.1016/J.IJMACHTOOLS.2008.10.015, 6.
[50] J. Sieniawski, K. Nadolny, Experimental study into the grinding force in surface grinding of steel CrV12 utilizing a zonal centrifugal coolant provision system, Proc. Inst. Mech. Eng. B J. Eng. Manuf. 232 (2016) 394–403, https://doi.org/10.1177/0954405416645256.
[51] M. Barmouz, B. Azarhoushang, A. Zahedi, F. Rabiei, F. Steinhäuser, Progress in grinding performance by additive manufacturing of grinding wheels integrated with internal venturi cooling channels and surface slots, J. Manuf. Process. 99 (2023) 485–500, https://doi.org/10.1016/J.JMAPRO.2023.05.078.
[52] R. Peng, W. Yan, L. Zhao, M. Chen, X. Xiao, Design and performance evaluation of a directional internal-cooling grooved grinding wheel with optimized coolant supply structure, J. Manuf. Process. 141 (2025) 155, https://doi.org/10.1016/J.JMAPRO.2025.02.059, 68.
[53] S. Costa, P. Capela, M.S. Souza, J.R. Gomes, L. Carvalho, M. Pereira, et al., A new grinding wheel design with a 3D internal cooling structure system, J. Manuf. Mater. Process. 8 (2024) 159, https://doi.org/10.3390/jmmp8040159.
[54] S. Costa, P. Capela, A. Hassui, J. Ribeiro, M. Pereira, D. Soares, CFD analysis of multi-layer cooling channels in three-dimensionally structured grinding wheels, Appl. Therm. Eng. 279 (2025) 127633, https://doi.org/10.1016/j.applthermaleng.2025.127633.
[55] S. Costa, A. Souza, L. Neves, J. Ribeiro, M. Pereira, D. Soares, Coolant flow in structured grinding wheels: CFD validation via high-speed imaging and particle tracking, Appl. Therm. Eng. (2025) 128689, https://doi.org/10.1016/j.applthermaleng.2025.128689.
[56] S. Malkin, C. Guo, Thermal analysis of grinding, CIRP Ann. 56 (2007) 760, https://doi.org/10.1016/j.cirp.2007.10.005, 82.
[57] S.D. Mihić, S. Cioc, I.D. Marinescu, M.C. Weismiller, Detailed study of fluid flow and heat transfer in the abrasive grinding contact using computational fluid dynamics methods, J. Manuf. Sci. Eng. 135 (2013), https://doi.org/10.1115/1.4023719/694803.
[58] M. Barmouz, F. Steinhäuser, B. Azarhoushang, Green grinding of ultra-high molecular weight polyethylene using glass fiber reinforced highly porous 3D-printed metal bond grinding wheel, Results Mater. 26 (2025) 100696, https://doi.org/10.1016/J.RINMA.2025.100696.